An Investigation of Phenomenal Parasitics and Robust Control of Parallel-Plate Electrostatic Micro Actuators

Guchuan Zhu[a], Jean-François Chianetta[b], Mehran Hosseini[b], and Yves-Alain Peter[b]

[a]Department of Electrical Engineering, École Polytechnique de Montréal,
C.P. 6079, Succursale centre-ville, Montreal, QC, Canada H3C 3A7
[b]Engineering Physics Department, École Polytechnique de Montréal,
C.P. 6079, Succursale centre-ville, Montreal, QC, Canada H3C 3A7

ABSTRACT

This paper extends the modeling of the effect of fringing field, proposed in our recent work,[1] to more generic devices: electrostatic parallel-plate actuators with deformations. Though these devices can be model as two parallel capacitors with a variable factor depending on the displacement,[2] it is difficult to determine the analytical expression of such a function. It is shown that, like the effect of fringing field, the modeling error of the effective actuator due to deformations can be compensated by introducing a variable serial capacitor. When a suitable robust control is used, the full knowledge of the introduced serial capacitor is not required, but merely its boundaries of variation. Based on this model, a robust control scheme is constructed using the theory of input-to-state stability (ISS) and backstepping state feedback design. This method allows loosening the stringent requirements on modeling accuracy without compromising the performance. The stability and the performance of the system using this control scheme are demonstrated through both stability analysis and numerical simulation.

Keywords: Phenomenal parasitics; modeling of electrostatic MEMS; FEM based simulation; input-to-state stability; robust nonlinear control.

1. INTRODUCTION

In the most popular model of electrostatic parallel-plate actuators, the moveable plate is supposed to be a rigid body without deformation and only the main electrical field (perpendicular to both electrodes) is considered. The capacitance of such structures is computed by

$$C = \frac{\epsilon A}{G(t)}, \tag{1}$$

where A is the area of electrodes, G the air gap, and ϵ the permittivity in the gap. This model is subject to modeling errors due to, e.g., deformations, fringing field effect, and parasitics related to the layout. Fabrication deviations and environmental fluctuations may also introduce parameter variations, affecting the reliability of the model.

The performance of the controller obtained from the simplified model might be compromised for applications where the precise positioning is required, e.g. adaptive optics.[3] To assure a high performance, one might want to use more accurate model. However, this might result in more complicated mathematical model and, consequently, make the control system difficult to implement and unreliable. For examples, modeling the fringing field and deformations leads in general to distributed parameter systems described by partial differential equations. The control of such systems requires distributed sensing and actuation, which is very hard to implement for microsystems.

We have proposed, in our recent work,[1] to model the effect of fringing field by a serial capacitor. Combined with an appropriate robust control, the full knowledge of the introduced serial capacitor is not required, but only its boundaries of variation, which can be obtained by simulations using off-the-shelf commercial software tools, e.g. ANSYS™, COMSOL™, and CoventorWare™, or by experimental measurements. This ideal considerably simplified the complexity of the model without compromising the performance of the control system. In this work, we will extend this method to

Further author information: (Send correspondence to G. Zhu or Y.-A. Peter)
G. Zhu: E-mail: guchuan.zhu@polymtl.ca
Y.-A. Peter: E-mail: yves-alain.peter@polymtl.ca

Optomechatronic Actuators, Manipulation, and Systems Control, edited by Yukitoshi Otani, Farrokh Janabi-Sharifi,
Proc. of SPIE Vol. 6374, 63740V, (2006) · 0277-786X/06/$15 · doi: 10.1117/12.692301

deformed structure and will shown that in the presence of deformation, the modeling error can also be compensated by introducing a suitable serial capacitor.

The robust control scheme used in this work is based on the theory of input-to-state stabilization (ISS) and back-stepping state feedback design. The nominal model used in control law design is the simplified parallel-plate actuator, but the controller is made robust against parasitics and parametric uncertainties. The stability and the performance of the system using this control scheme are demonstrated through both stability analysis and numerical simulation.

The rest of the paper is organized as follows. Section 2 models the capacitance of 1DOF parallel-plate electrostatic actuator in the presence of deformation. Section 3 is devoted to the construction of control law. The simulation results are reported in Section 4 and Section 5 contains some concluding remarks.

2. MODELING OF PARALLEL-PLATE ELECTROSTATIC MICRO ACTUATORS IN THE PRESENCE OF PHENOMENAL PARASITICS

2.1. Modeling of Ideal Devices

Denote by m the weight of the moveable plate, by k the elastic constant of the suspension beams, and by b the damping coefficient of the structure. The equation of motion of the actuator is then given by

$$m\ddot{G}(t) + b\dot{G}(t) + k(G(t) - G_0) = F(t), \tag{2}$$

where G_0 is the zero voltage gap and $F(t)$ the force due to electrical field.

Let $Q(t)$ be the charge on the device and $V_a(t)$ the actuation voltage. One can deduced from the capacitance (1) the electrostatic force of ideal parallel-plate actuator which reads

$$F(t) = \frac{V_a^2}{2}\frac{\partial C}{\partial G} = -\frac{\epsilon A V_a^2}{2G^2(t)} = -\frac{Q^2(t)}{2\epsilon A}. \tag{3}$$

Note that the electrostatic force is always attractive regardless of the polarization of the control signal.

Assuming the system started operating from an initially uncharged state at $t = 0$, then the charge on the electrodes at the time t is:

$$Q(t) = \int_0^t I_s(\tau)d\tau, \tag{4}$$

or equivalently

$$\dot{Q}(t) = I_s(t), \tag{5}$$

where $I_s(t)$ is the source current through the loop resistor R. By a simple application of Kirchhoff's Voltage Law we obtain:[4]

$$\dot{Q}(t) = \frac{1}{R}\left(V_s(t) - \frac{Q(t)G(t)}{\epsilon A}\right), \tag{6}$$

where $V_s(t)$ is the source voltage, which is the actual control variable.

2.2. Capacitance Model of Deformed Devices

When deformation happens, the displacement is no longer uninform: the center portion is largest whereas the portions near the step-up supports hardly move at all. The deformed device can be modeled as the sum of two onedimensional (1-D) capacitances: a variable capacitor, representing the effective actuator, in parallel with another one whose equivalent surface is parameterized by the air gap, as shown in Fig. 1. The total capacitance of such devices can be expressed as:[2]

$$C = C_a + C_p \propto \frac{1-\gamma}{G} + \frac{\gamma}{G_0}, \tag{7}$$

where C_a is the capacitance of the actuator, C_p is the the capacitance of the parallel capacitor, and γ is a proper function that increases as the gap closes.

To illustrate the effect of deformation, we have simulated a micro structure using finite element methods (FEM) based MEMS CAD software package Coventorware™. The electrodes are square of 206×206 μm^2 and the moveable plate is

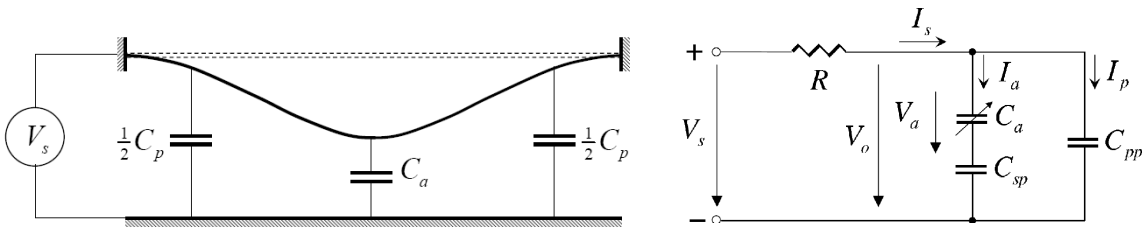

Figure 1. Schematic representation of the deformed structure and its equivalent circuit.

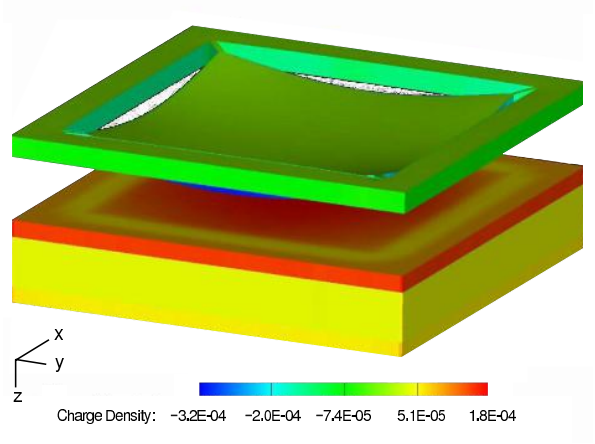

Figure 2. FEM based simulation of a deformed micro-structure.

sustained by four beams clamped at the corners. The thickness of the moveable plate is 1.5088μm and the initial gap is 5μm. The deformation and the distribution of charge density at a position of deflection is shown in Fig. 2. The capacitance of the device obtained from CoventorWare^{TM} simulation and the one calculated from the rigid body approximation (1) are given in Table 1. It can be seen that for small deflections, the deformation is not significant and the capacitance of the simulated device is higher than the one calculated from the rigid body approximation (about 17% higher at the zero voltage position). This is due to the unmodeled phenomena, e.g., the effect of fringing field. For large deflections, the deformation becomes important. In this case, the capacitance calculated from (1) is overestimated. For a deflection of 4.8431 μm, the modeling error can be as high as 47%. Note that the effect of fringing field decreases as the gap closes. Therefore, the modeling error for large deflections is mainly due to the deformation.

Obviously, it is very difficult to determining the function γ in (7), because it changes with the structure, the geometry, and the material of the actuator. To overcome this difficulty, we adopted the method developed in our recent work[1] by modeling the device as an ideal rigid body, called also the nominal structure, combined with an appropriate variable serial capacitor. The capacitance of the nominal structure, C_a, follows the ideal model (1), but uses an effective area A_{eff} to compensate the modeling errors at the zero voltage position. Since the deformation has effect of decreasing the capacitance and the effect of fringing field is maximum at the initial gap, the nominal structure gives overestimated capacitance for any non zero deflection. The introduced serial capacitor has the effect of reducing the total capacitance and, hence, it will eliminate the modeling error. The value of the introduced serial capacitor is a function of the gap and can be expressed as

$$\frac{1}{C_{sp}} = \frac{1}{C_{real}} - \frac{1}{C_a}. \tag{8}$$

Obviously, since C_{real} is unknown, one can not determine C_{sp}. However, as mentioned earlier, for an appropriate robust control scheme, the full knowledge of the relationship between serial capacitance and deflection is not required, but only its variation boundaries.

Table 1. Capacitances for different deflections.

Deflection (μm)	Capacitance (pF)	
	FEM Simulation	Rigid Body Approximation
0	0.0909	0.0751
0.6459	0.1004	0.0863
1.1798	0.1103	0.0983
1.9488	0.1292	0.1231
2.4944	0.1485	0.1499
3.1086	0.1811	0.1986
3.5897	0.2220	0.2663
4.1133	0.3049	0.4236
4.5522	0.4973	0.8386
4.7492	1.0253	1.4972
4.8431	1.6286	2.3934

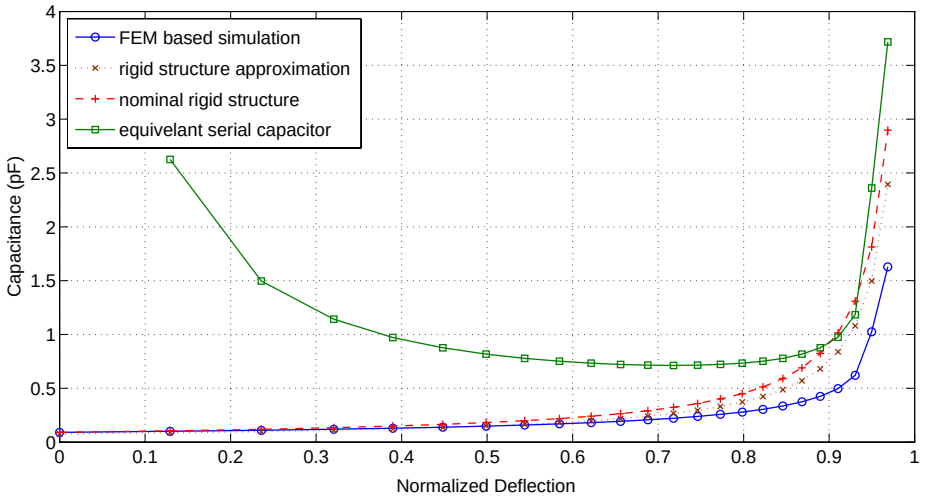

Figure 3. Capacitance of the simulated device, the rigid structure approximation, the nominal structure, and the introduced serial capacitor.

Figure 3 shows the capacitance of the simulated device, the rigid body approximation, and the nominal structure. The introduced serial capacitor is computed from (8) using the capacitances of the simulated device and the nominal structure. The value of the nominal capacitor at the initial gap is equal to 0.0909 pF (the same as the real capacitor at this position). Except for the initial separation gap, there is a difference between the value of nominal capacitor and the real one. The role of the serial capacitor is to compensate this difference. As shown in Fig. 3, this serial capacitance is infinite at the initial gap and has a minimum that is about 0.7126 pF for this structure. Since the smaller the introduced serial capacitance, the bigger the influence of modeling errors, we can use this value to determine the boundary of the introduced serial capacitor in the model.

As the introduced serial capacitor and the parallel capacitor due to the deformation are essentially unknown, following the terminology of Ref. 2, we can call them phenomenal parasitics. Obviously, the effect of fringing field can also be considered as serial parasitics.[1] A generic capacitance model of the deformed parallel-plate is given in Fig. 1, in which C_{pp} is composed of different unmodeled parallel capacitors due to, e.g., the deformation and the layout.

2.3. Dynamics of the Actuator in the Presence of Parasitics

When taking into account for parasitics, the dynamic equation of the electrical subsystem is given by[1]

$$\dot{Q}_a(t) = \frac{1}{R\left(1+\rho_p\rho_s+\rho_p\dfrac{G}{G_0}\right)}\left(V_s - \left(\frac{G}{\epsilon A}+\rho_s\frac{G_0}{\epsilon A}+R\rho_p\frac{\dot{G}}{G_0}\right)Q_a\right), \tag{9}$$

where

$$\rho_p = \frac{C_{pp}}{C_0},\ \ \rho_s = \frac{C_0}{C_{sp}},$$

with $C_0 = \epsilon A_{eff}/G_0$, the capacitance of the nominal structure at the initial gap G_0.

In our modeling, ρ_p and ρ_s represent the influence of parasitics. When their value is set to zero, the dynamics of the electrical subsystem will be reduced to the one for ideal devices given in (6).

It can be seen from (9) that the parallel parasitic capacitance will not change the static behavior of the device. However, the dynamics of the electrical subsystem will be affected: the bigger the parallel parasitic capacitance, the slower the dynamics of the driving circuit. Consequently, the performance of the system will be degraded if the parallel parasitic capacitance is not taken into account in the design of the control system. The serial parasitic capacitance will affect both the static and the dynamic behavior of the system. It is straightforward to show that the serial parasitic capacitance will change the position of pull-in.

Note that since the nominal plan is an ideal rigid body, the mechanical subsystem still follows (2) with electrostatic force given in (3). Therefore the parasitics affect only the dynamics of the electrical subsystem.

To make the system analysis and control design easier, we transform (2) and (9) into normalized coordinates by changing the time scale, $\tau = \omega_0 t$, and performing a normalization as follows:[5]

$$x = 1-\frac{G}{G_0},\ q=\frac{Q_a}{Q_{pi}},\ u=\frac{V_s}{V_{pi}},\ i=\frac{I_s}{V_{pi}\omega_0 C_0},\ r=\omega_0 C_0 R,$$

where $V_{pi} = \sqrt{8kG_0^2/27C_0}$ is the nominal pull-in voltage, $Q_{pi} = \frac{3}{2}C_0V_{pi}$ the nominal pull-in charge, $\omega_0 = \sqrt{k/m}$ the undamped natural frequency, and $\zeta = b/2m\omega_0$ the damping ratio. We then have

$$\frac{dq}{d\tau} = \frac{1}{r\left(1+\rho_p(1-x)+\rho_p\rho_s\right)}\left(\frac{2}{3}u-(1-x)q-\rho_s q+r\rho_p q\frac{dx}{d\tau}\right). \tag{10}$$

Let $x_1 = x$, $x_2 = v$, and $x_3 = q^2$. System (2)-(10) can then be written in the normalized coordinates as

$$\frac{dx_1}{d\tau} = x_2 \tag{11a}$$

$$\frac{dx_2}{d\tau} = -2\zeta x_2 - x_1 + \frac{1}{3}x_3 \tag{11b}$$

$$\frac{dx_3}{d\tau} = \beta\left(\frac{4\sqrt{x_3}}{3}u - 2(1-x_1)x_3 - 2\rho_s x_3 + 2r\rho_p x_2 x_3\right) \tag{11c}$$

where

$$\beta = \frac{1}{r\left(1+\rho_p(1-x)+\rho_p\rho_s\right)} \tag{12}$$

is a function of deflection. System (11) is defined on the state space $\mathcal{X} = \left\{(x_1,x_2,x_3)\subset\mathbb{R}^3 \mid x_1\le 1,\ x_3\ge 0\right\}$.

Note that the considered actuator exhibits switching behavior. First of all, when the moveable plate hits the fixed one ($x_1 = 1$), the dynamics of the mechanical subsystem collapse.[6] In addition, $q = 0$ ($x_3 = 0$) is a singular point at which System (11) is not linearly controllable (see, e.g., Ref. 6). However, it is easy to see that the system is symmetric except for the sign of the charge. For simplicity, we ignore the contact dynamics and consider only the branch defined by (11c). Consequently, the stability property obtained through the proposed control will hold locally.

Since in what follows we deal only with normalized quantities, we can use t to denote the time and omit the qualifier "normalized."

3. ROBUST CONTROL DESIGN

3.1. Preliminaries of input-to-state stability

The concept of input-to-state stability is introduced by Sontag[7] and ISS-based design is a popular tool in the field of system control. We present here only the notations required in the development of the control law. The interested reader is referred to, for example, Ref. 8, 9 for a formal presentation.

The following comparison functions are required for presenting the method of input-to-state stabilization. A function $\alpha : [0, a) \to [0, \infty)$ is said to belong to class-$\mathcal{K}$ if it is continuous, strictly increasing, and $\alpha(0) = 0$. If $a = \infty$ and α is unbounded, the function is said to belong to $\mathcal{K}_\infty$. A function $\beta : [0, a) \times [0, \infty) \to [0, \infty)$ is said to belong to $\mathcal{KL}$ if it is nondecreasing in its first argument, nonincreasing in its second argument, and $\lim_{s\to 0^+} \beta(s, t) = \lim_{t\to\infty} \beta(s, t) = 0$.

The system

$$\dot{x} = f(x, u) \tag{13}$$

is said to be input-to-state stable if for any $x(0)$ and for any input $u(\cdot)$ continues and bounded on $[0, \infty)$ the solution exists for all $t \geq 0$ and satisfies

$$|x(t)| \leq \beta(x(0), t) + \gamma\left(\sup_{0\leq\tau\leq t} u(|\tau|)\right), \quad \forall t \geq 0, \tag{14}$$

where $\beta(s, t) \in \mathcal{KL}$ and $\gamma(s) \in \mathcal{K}$.

System (13) is ISS if and only if there exists a smooth positive define radially unbounded function V and class $\mathcal{K}_\infty$ functions α_1 and α_2 such that the time derivative of V along the solutions of (13) verifies

$$\dot{V} = \frac{\partial V}{\partial x} f(x, u) \leq -\alpha_1(|x|) + \alpha_2(|u|). \tag{15}$$

The function V satisfying the above inequality is called ISS-Lyapunov function.

Note that the method of ISS provides a convenient framework for robust system control, which amounts to finding a control with which the closed-loop system is stable with respect to the disturbances, considered now as the inputs to the system.

3.2. Control synthesis

In this work, we consider both the parasitics and parametric uncertainties, such as the variations of damping coefficient and loop resistance. We make then the following assumptions on the uncertainties in System (11).

ASSUMPTION 1. *The parasitic capacitances are bounded by known constants:*

$$0 \leq \rho_p \leq \bar{\rho}_p, \quad 0 \leq \rho_s \leq \bar{\rho}_s. \tag{16}$$

ASSUMPTION 2. *The damping ratio is positive and bounded and can be written as:*

$$\zeta = \zeta_0 + \Delta\zeta, \tag{17}$$

where ζ_0 is positive-valued representing the nominal damping ratio and $\Delta\zeta$ the modeling error.

ASSUMPTION 3. *The upper and lower bounds of the resistance in the loop, r, are known:*

$$0 < \underline{r} \leq r \leq \overline{r}. \tag{18}$$

Since $x_1 \leq 1$, β in (12) may be bounded as follows:

$$0 < \underline{\beta} \leq \beta \leq \overline{\beta}, \tag{19}$$

where $\overline{\beta} = 1/\underline{r}$. Note that since the electrostatic force is always attractive, the control allowing the moveable plate to move as far as possible beyond the initial gap is the one that can remove the charge from the device in an arbitrary small

time interval. However there is no equilibrium beyond the zero voltage gap and the mechanical subsystem (11-a)-(11-b) globally exponentially converges to the origin with zero input ($x_3 = 0$).[10] This implies that x_1 should not be smaller than -1. Therefore, in a normal operational condition, β should be lower bounded by

$$\underline{\beta} = \frac{1}{\overline{r}\left(1 + \overline{\rho}_p\left(2 + \overline{\rho}_s\right)\right)}. \tag{20}$$

Furthermore, the variation of β is denoted by

$$|\beta - \beta_0| \leq \overline{\beta} - \underline{\beta} \triangleq \Delta\beta. \tag{21}$$

where β_0 is the nominal value of β.

In this work, we will consider the tracking problem with $y = x_1$ as the output. Following a classical approach, we choose a sufficiently smooth reference trajectory y_r for x_1 as a function of time and then make this trajectory attractive.

A recursive procedure, called also backstepping design (see, e.g., Ref. 9 for a detailed presentation of this technique), is used in the design of the control law, which consists of, for System (11), the following three steps.

Step 1. Consider the control of the subsystem (11a) with x_2 as a virtual input. Let $z_1 = x_1 - y_r$ be the position tracking error and select a Lyapunov-like function

$$V_1 = \frac{1}{2}z_1^2.$$

The time derivative of V_1 along the solutions of (11.a) is

$$\dot{V}_1 = z_1(x_2 - \dot{y}_r).$$

The desired input (also called stabilizing function) can be chosen as:

$$x_{2d} = \dot{y}_r - k_1 z_1, \quad k_1 > 0. \tag{22}$$

Step 2. Consider now the subsystem (11a)-(11b) with x_3 as a virtual input. Define $z_2 = x_2 - x_{2d}$ and augment V_1 to yield:

$$V_2 = V_1 + \frac{1}{2}z_2^2.$$

Letting $z_3 = x_3 - x_{3d}$, the time derivative of V_2 along the solutions of the corresponding subsystem is given by

$$\begin{aligned}\dot{V}_2 =& -k_1 z_1^2 + z_2\left(z_1 + \dot{x}_2 - \dot{x}_{2d}\right)\\ =& -k_1 z_1^2 + z_2\left(z_1 - 2(\zeta_0 + \Delta\zeta)x_2 - x_1 + \frac{1}{3}(z_3 + x_{3d}) - \dot{x}_{2d}\right).\end{aligned}$$

In order to counteract the uncertainty $\Delta\zeta$, a nonlinear damping term should be added to the stabilizing function. The desired input in this case is of the following form:

$$x_{3d} = 3\left(2\zeta_0 x_2 + x_1 + \dot{x}_{2d} - z_1 - \kappa_2\zeta_0 x_2^2 z_2 - k_2 z_2\right), \tag{23}$$

where $k_2 > 0$ and κ_2 is the gain of the nonlinear damping term, the lower bound of which will be given latter on.

Step 3. Finally the Lyapunov function candidate for System (11) is chosen to be

$$V_3 = V_2 + \frac{1}{2}z_3^2 = \frac{1}{2}z_1^2 + \frac{1}{2}z_2^2 + \frac{1}{2}z_3^2$$

whose time derivative along the solutions of System (11) is given by

$$\begin{aligned}\dot{V}_3 =& -k_1 z_1^2 - k_2 z_2^2 - 2\Delta\zeta x_2 z_2 - \kappa_2\zeta_0 x_2^2 z_2^2 + z_3\left(\frac{z_2}{3} - 3(ab_1 + b_2) + 6\Delta\zeta b_1 x_2\right.\\ &\left. + \beta\left(\frac{4\sqrt{x_3}}{3}u - 2x_3(1 - x_1) + 2r\rho_p x_2 x_3 - 2\rho_s x_3\right)\right)\end{aligned} \tag{24}$$

where

$$\begin{aligned} a =& -2\zeta_0 x_2 - x_1 + \frac{1}{3}x_3, \\ b_1 =& 2\zeta_0 - k_1 - k_2 - \kappa_2\zeta_0\left(2x_2 z_2 + x_2^2\right), \\ b_2 =& y_r^{(3)} + k_1\ddot{y}_r + \dot{y}_r + \left(\kappa_2\zeta_0 x_2^2 + k_2\right)\dot{x}_{2d}. \end{aligned}$$

Let $U = \frac{4}{3}\sqrt{x_3}u$. The proposed backstepping controller is given by:

$$\begin{aligned} U =& 2x_3(1-x_1) + \frac{3}{\underline{\beta}}\left(ab_1 + b_2 - \frac{z_2}{9}\right) - \frac{1}{\underline{\beta}}k_3 z_3 - \frac{1}{\underline{\beta}}\kappa_{31}\left(ab_1 + b_2 - \frac{z_2}{9}\right)^2 z_3 - \frac{1}{\underline{\beta}}\kappa_{32}\zeta_0 b_1^2 x_2^2 z_3 \\ & - \frac{1}{\underline{\beta}}\kappa_{33}x_2^2 x_3^2 z_3 - \frac{1}{\underline{\beta}}\kappa_{34}x_3^2 z_3 \end{aligned} \tag{25}$$

with $k_3 > 0$, where κ_{31}, κ_{32}, κ_{33}, and κ_{34} are the gains of the nonlinear damping terms.

THEOREM 3.1. *For System (11) with the uncertainties satisfying Assumptions 1-3 and y_r being sufficiently smooth, the backstepping controller (25) with*

$$\kappa_2 > \frac{1}{2\zeta_0},\ \kappa_{31} > 1,\ \kappa_{32} > \frac{1}{\zeta_0},\ \kappa_{33} > 1,\ \ \kappa_{34} > \frac{1}{\underline{r}^2}, \tag{26}$$

renders the closed-loop error dynamics locally ISS with respect to the uniformly bounded inputs $\Delta\beta$, ρ_p, ρ_s, and $\Delta\zeta$. Furthermore, the ultimate bound for the tracking error z_1 can be rendered arbitrarily small by picking the feedback gains k_1, k_2, and k_3 large enough.

The proof the the above theorem is given in Appendix A.

Note that the actual control u is singular when $x_3 = 0$. This is due to the uncontrollability of System (11) at the zero voltage position. However this situation happens only at this point. It is easy to see that System (11) is stabilizing at this position with an input $u = 0$. By defining an open ball $B_\varepsilon = \{X | \|X\| < \varepsilon\} \subset \mathcal{X}$ of radius ε centered at the origin, where $X = (x_1, x_2, x_3)^T$ and $\|\cdot\|$ the usual Euclidean norm, a more practical control law can be expressed as

$$u = \begin{cases} \dfrac{3}{4\sqrt{x_3}}U, & \text{for } X \notin B_\varepsilon \\ 0, & \text{for } X \in B_\varepsilon \end{cases} \tag{27}$$

where U is given by (25).

3.3. Reference Trajectory Design

In general, reference trajectories can be chosen to be any sufficiently smooth function $t \mapsto y(t)$, connecting the initial point at time t_i to a desired point at time t_f, such that the initial and final conditions are verified. The reference trajectory used in our control schemes is a polynomial of the following form:

$$y_r(t) = y(t_i) + (y(t_f) - y(t_i))\tau^5(t)\sum_{i=0}^{4} a_i\tau^i(t), \tag{28}$$

where $\tau(t) = (t - t_i)/(t_f - t_i)$. For a set-point control, the coefficients in (28) can be determined by imposing the initial and final conditions

$$\dot{y}(t_i) = \dot{y}(t_f) = \ddot{y}(t_i) = \ddot{y}(t_f) = y^{(3)}(t_i) = y^{(3)}(t_f) = 0,$$

which yield $a_0 = 126$, $a_1 = -420$, $a_2 = 540$, $a_3 = -315$, and $a_4 = 70$.

The polynomial in (28) is one of the most used reference trajectories in flatness based control. A more general formulation can be found in Ref. 11.

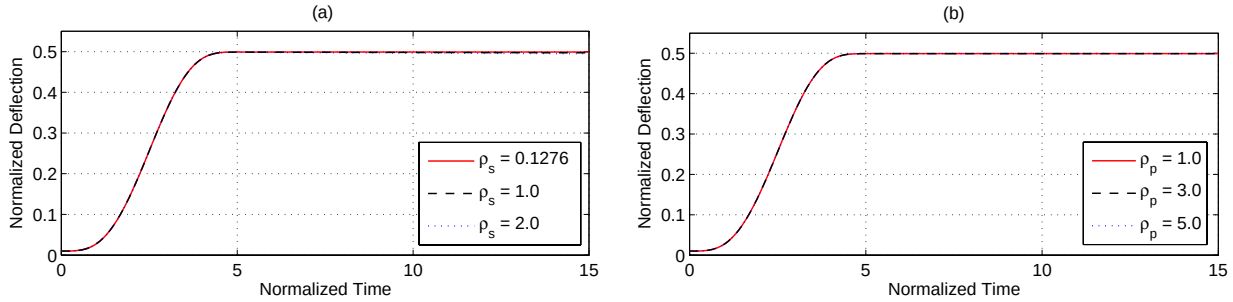

Figure 4. Influence of parasitics: (a) variation of serial parasitics ρ_s; (b) variation of parallel parasitics ρ_p.

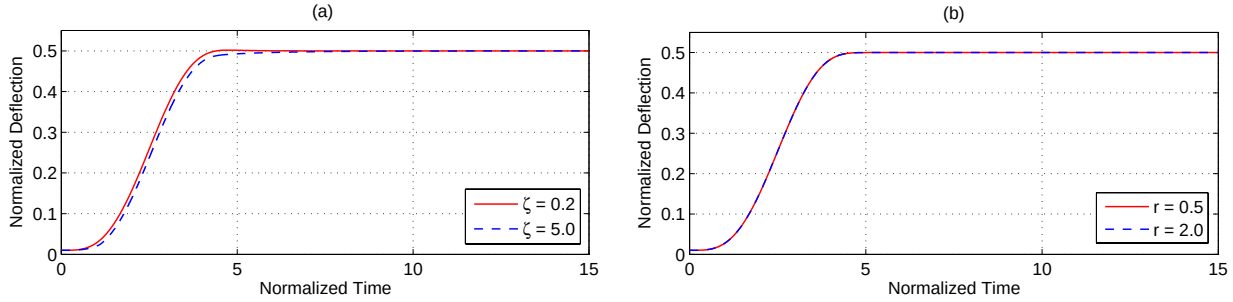

Figure 5. Robustness against parametric uncertainties: (a) variation of damping coefficient ζ; (b) variation of resistance in the loop r.

4. SIMULATION STUDY

In our simulation study, the parameters of the nominal plant are $\zeta_0 = 1$, $r_0 = 1$, $\rho_p = 0$, and $\rho_s = 0$. The actuator is supposed to be driven by a bipolar voltage source. The boundaries of parasitics and parametric uncertainties are fixed to be $\overline{\rho}_s = 2$, $\overline{\rho}_p = 5$, $\overline{r} = 2$, and $\underline{r} = 0.5$. We have then $\underline{\beta} = 0.0238$. Note that a small bias voltage is applied to the device in order to avoid the singularity at the origin.

Firstly we consider only the influence of the parasitics. Based on the simulation in Section 2.2 we have for the device considered $\rho_{s_{max}} = 0.1276$. Therefore $\overline{\rho}_s >> \rho_{s_{max}}$ and the tested system should support more important modeling errors. It can be seen from Fig. 4 that in the simulated range of variation of the parasitics, the system performs nearly identically.

The second test is concerned with the uncertainties in the damping coefficient ζ and the resistance in the loop r. It is shown (see Fig. 5) that the system still performs very well even for very important parameter variations.

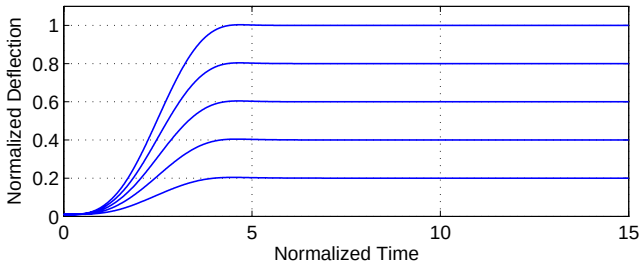

Figure 6. Simulation results of set-point control.

In the last test, we simulated the system for set-point control. The parameters for the simulated system are chosen as $\rho_s = 0.1276$, $\rho_p = 1.0$, $\zeta = 0.5$, and $r = 1.5$. It can be seen from Fig. 6 that the performance of the system is quite uniform for different deflections.

Note that the performance of the controller presented in this work is quite similar to the one obtained by cascade ISS synthesis proposed in our previous work.[1]

5. CONCLUSIONS

This paper considered the effect of deformation of the moveable plate of parallel-plate electrostatic micro-actuators and extended the idea of introducing a variable serial capacitor to compensate modeling errors due to deformation. Combined with an appropriate robust control scheme, the exact analytical expression of the serial capacitance is not required, but merely its boundary represented by the ratio of its minimal value and the equivalent nominal capacitance at the initial position. CoventorWare™ has been used to estimate the variation range of the introduced serial capacitor for a micro-structure. A state feedback robust control scheme using the technique of ISS and backstepping design is constructed and the closed-loop stability of the system is demonstrated. Numerical simulations show that the proposed control system has satisfactory performance and robustness vis-à-vis parasitics and parametric uncertainties. It has been shown that presenting different type of modeling errors by parasitics, using numerical simulation or experimental measurements to determine the variation boundaries of parasitics, and then employing robust control techniques will considerably simplify the modeling of micro-devices. Obviously, this idea can be applied to micro-devices with more complex structure for which building accurate model is a very challenging task.

APPENDIX A. PROOF OF THEOREM 3.1

Substituting the input in (24) by the backstepping controller (25) and taking into account the bounds (16), (18), and (19) yields

$$\begin{aligned}
\dot{V}_3 =& -k_1 z_1^2 - k_2 z_2^2 - 2\Delta\zeta x_2 z_2 - 2\kappa_2\zeta_0 x_2^2 z_2^2 + z_3\left(-\frac{\beta}{\underline{\beta}}k_3 z_3 + 3\left(\frac{\beta}{\underline{\beta}}-1\right)\left(ab_1+b_2-\frac{z_2}{9}\right)\right.\\
&-\frac{\beta}{\underline{\beta}}\kappa_{31}\left(ab_1+b_2-\frac{z_2}{9}\right)^2 z_3 + 6\Delta\zeta x_2 b_1 - \frac{\beta}{\underline{\beta}}\kappa_{32}\zeta_0 b_1^2 x_2^2 z_3 + 2\beta\rho_p r x_2 x_3 - \frac{\beta}{\underline{\beta}}\kappa_{33}x_2^2 x_3^2 z_3\\
&\left.-2\beta\rho_s x_3 - \frac{\beta}{\underline{\beta}}\kappa_{34}x_3^2 z_3\right)\Big)\\
=& -k_1 z_1^2 - k_2 z_2^2 - \frac{\beta}{\underline{\beta}}k_3 z_3^2 - 2\Delta\zeta x_2 z_2 - 2\kappa_2\zeta_0 x_2^2 z_2^2 + 3\frac{\beta-\underline{\beta}}{\underline{\beta}}\left(ab_1+b_2-\frac{z_2}{9}\right)z_3 - \frac{\beta}{\underline{\beta}}\kappa_{31}\left(ab_1+b_2-\frac{z_2}{9}\right)^2 z_3^2\\
&+6\Delta\zeta x_2 b_1 z_3 - \frac{\beta}{\underline{\beta}}\kappa_{32}\zeta_0 b_1^2 x_2^2 z_3^2 + 2\beta\rho_p r x_2 x_3 z_3 - \frac{\beta}{\underline{\beta}}\kappa_{33}x_2^2 x_3^2 z_3^2 - 2\beta\rho_s x_3 z_3 - \frac{\beta}{\underline{\beta}}\kappa_{34}x_3^2 z_3^2. \qquad (29)
\end{aligned}$$

Applying Young's inequality and noting that $\beta \geq \underline{\beta}$ and

$$\beta r \leq \frac{1}{1+\rho_p(2+\rho_s)},$$

the last expression can be bounded as follows

$$\begin{aligned}
\dot{V}_3 \leq& -k_1 z_1^2 - k_2 z_2^2 - k_3 z_3^2 - (2\kappa_2\zeta_0 - 1)x_2^2 z_2^2 - \left(\kappa_{31}\frac{\beta}{\underline{\beta}}-1\right)\left(ab_1+b_2-\frac{z_2}{9}\right)^2 z_3^2 - \left(\kappa_{32}\zeta_0\frac{\beta}{\underline{\beta}}-1\right)b_1^2 x_2^2 z_3^2\\
&-\left(\frac{\beta}{\underline{\beta}}\kappa_{33}-1\right)x_2^2 x_3^2 z_3^2 - \left(\frac{\beta}{\underline{\beta}}\kappa_{34}-\frac{1}{\underline{r}^2}\right)x_3^2 z_3^2 + 10\Delta\zeta^2 + \frac{\rho_p^2+\rho_s^2}{(1+\rho_p(2+\rho_s))^2} + \frac{9}{4}\Delta\beta^2. \qquad (30)
\end{aligned}$$

If (26) is satisfied, then

$$\dot{V}_3 \leq -\alpha(z) + 10\Delta\zeta^2 + \frac{\rho_p^2+\rho_s^2}{(1+\rho_p(2+\rho_s))^2} + \frac{9}{4}\Delta\beta^2 \qquad (31)$$

where

$$\alpha(z) = -k_1 z_1^2 - k_2 z_2^2 - k_3 z_3^2$$

is obviously a class $\mathcal{K}_\infty$ function. Noting that $(\rho_p^2 + \rho_s^2)/(1 + \rho_p(2 + \rho_s))^2$ is uniformly bounded, the closed-loop error dynamics are thus ISS with $\Delta\zeta$, ρ_p, ρ_s, and $\Delta\beta$ as the inputs.

REFERENCES

1. M. Hosseini, G. Zhu, and Y.-A. Peter, "A new formulation of fringing capacitance and its application to the control of parallel-plate electrostatic micro actuators," in *2006 DTIP of MEMS & MOEMS*, pp. 211–216, (Stresa, Italy), 26-28 April 2006.
2. E. Chan and R. Dutton, "Electrostatic micromechanical actuator with extended range of travel," **9**, pp. 321–328, Spet. 2000.
3. N. Doble and D. Williams, "The application of MEMS technology for adaptive optics in vision science," *IEEE J. Select. Topics Quantum Electron.* **10**, pp. 629–635, May/June 2004.
4. S. Senturia, *Microsystem Design*, Kluwer Academic Publishers, Norwell, MA, 2002.
5. J. Pont-Nin, A. Rodríguez, and L. Castañer, "Voltage and pull-in time in current drive of electrostatic actuators," **11**(3), pp. 196–205, 2002.
6. D. H. S. Maithripala, J. M. Berg, and W. P. Dayawansa, "Control of an electrostatic MEMS using static and dynamic output feedback," *ASME Journal of Dynamic Systems, Measurement and Control* **127**, pp. 443–450, 2005.
7. E. Sontag, "Smooth stabilization implies coprime factorization," **34**, pp. 435–443, 1989.
8. E. Sontag, "The ISS philosophy as a unifying framework for stability-like behavior," in *Nonlinear Control in the Year 2000 (Volume 2)*, A. Isidori, F. Lamnabhi-Lagarrigue, and W. Respondek, eds., *Lecture Notes in Control and Information Sciences*, pp. 443–468, Springer-Verlag, Berlin, 2000.
9. M. Krstić, I. Kanellakopoulos, and P. Kokotović, *Nonlinear and Adaptative Control Design*, John Wiley & Sons Ltd, New York, 1995.
10. D. Maithripala, J. Berg, and W. Dayawansa, "Nonlinear dynamic output feedback stabilization of electostatically actuated MEMS," in *Proc. of the 42nd IEEE Conference on Decision and Control*, pp. 61–66, (Maui, Hawaii), December 2003.
11. J. Lévine, *Analyse et Commande des Systmes Non Linaires*, [Online] Available: http://cas.ensmp.fr/%7Elevine/Enseignement /CoursENPC.pdf, 2004.